Physics of Plasmas

Perturbation modifications by pre-magnetisation of inertial confinement fusion implosions

Cite as: Phys. Plasmas **26**, 022701 (2019); https://doi.org/10.1063/1.5085498
Submitted: 13 December 2018 . Accepted: 21 December 2018 . Published Online: 01 February 2019

C. A. Walsh, K. McGlinchey, J. K. Tong, B. D. Appelbe, A. Crilly, M. F. Zhang, and J. P. Chittenden

COLLECTIONS

This paper was selected as an Editor's Pick

View Online Export Citation CrossMark

ARTICLES YOU MAY BE INTERESTED IN

Deep learning: A guide for practitioners in the physical sciences
Physics of Plasmas **25**, 080901 (2018); https://doi.org/10.1063/1.5020791

Robustness to hydrodynamic instabilities in indirectly driven layered capsule implosions
Physics of Plasmas **26**, 012707 (2019); https://doi.org/10.1063/1.5080262

Scaling laws for dynamical plasma phenomena
Physics of Plasmas **25**, 100501 (2018); https://doi.org/10.1063/1.5042254

© 2019 Author(s).

Physics of Plasmas ARTICLE scitation.org/journal/php

Perturbation modifications by pre-magnetisation of inertial confinement fusion implosions

Cite as: Phys. Plasmas **26**, 022701 (2019); doi: 10.1063/1.5085498
Submitted: 13 December 2018 · Accepted: 21 December 2018 · Published Online: 01 February 2019

View Online Export Citation CrossMark

C. A. Walsh,[a),b)] K. McGlinchey, J. K. Tong, B. D. Appelbe, A. Crilly, M. F. Zhang, and J. P. Chittenden

AFFILIATIONS

Blackett Laboratory, Imperial College, London SW7 2AZ, United Kingdom

Note: This paper is part of the Special Collection: Papers from the 60th Annual Meeting of the APS Division of Plasma Physics.
Note: Paper NI2 3, Bull. Am. Phys. Soc. **63** (2018).
[a)] Invited speaker.
[b)] **Electronic mail:** c.walsh14@imperial.ac.uk

ABSTRACT

Pre-magnetisation of inertial confinement fusion implosions on the National Ignition Facility has the potential to raise current high-performing targets into the ignition regime [Perkins *et al.* "The potential of imposed magnetic fields for enhancing ignition probability and fusion energy yield in indirect-drive inertial confinement fusion," Phys. Plasmas **24**, 062708 (2017)]. A key concern with this method is that the application of a magnetic field inherently increases asymmetry. This paper uses 3-D extended-magnetohydrodynamics Gorgon simulations to investigate how thermal conduction suppression, the Lorentz force, and α-particle magnetisation affect three hot-spot perturbation scenarios: a cold fuel spike, a time-dependent radiation drive asymmetry, and a multi-mode perturbation. For moderate magnetisations ($B_0 = 5$ T), the single spike penetrates deeper into the hot-spot, as thermal ablative stabilisation is reduced. However, at higher magnetisations ($B_0 = 50$ T), magnetic tension acts to stabilise the spike. While magnetisation of α-particle orbits increases the peak hot-spot temperature, no impact on the perturbation penetration depth is observed. The P4-dominated radiation drive asymmetry demonstrates the anisotropic nature of the thermal ablative stabilisation modifications, with perturbations perpendicular to the magnetic field penetrating deeper and perturbations parallel to the field being preferentially stabilised by increased heat-flows. Moderate magnetisations also increase the prevalence of high modes, while magnetic tension reduces vorticity at the hot-spot edge for larger magnetisations. For a simulated high-foot experiment, the yield doubles through the application of a 50 T magnetic field-an amplification which is expected to be larger for higher-performing configurations.

Published under license by AIP Publishing. https://doi.org/10.1063/1.5085498

I. INTRODUCTION

Inertial confinement fusion (ICF) experiments at the National Ignition Facility (NIF) are hampered by asymmetries,[2] resulting in larger cooling of the hot fuel core (hot-spot) than anticipated. While the majority of current research efforts at NIF are directed at understanding and controlling the growth of these asymmetries, an alternate route accepts that perturbations are unavoidable in ICF experiments and instead reduces hot-spot cooling through the application of external magnetic fields.[3,4] An externally applied magnetic field of 5 T can be compressed by the imploding capsule to intensities greater than 3000 T, as inferred using a cylindrical target on the OMEGA Laser Facility.[5] Similar spherical capsule implosion experiments then observed a 15% increase in the hot-spot temperature and a 30% increase in the neutron yield due to thermal conduction magnetisation from an initial magnetic field of 8 T.[4] 2-D magnetohydrodynamics (MHD) simulations expect a 50 T magnetic field to bring the current high-performing NIF experiments into the ignition regime.[1,6] However, imposed magnetic fields seed additional asymmetries onto the capsule,[1] and the integrated effect of plasma magnetisation on 3-D perturbation growth remains an area for investigation.

The dominant impact of magnetic fields on these capsule implosions can be split into three components:

- Electron heat-flow magnetisation,
- Lorentz force,
- α-particle trapping.

Published under license by AIP Publishing

This paper demonstrates the varying impact of these magnetisation effects on the shape of pre-magnetised ICF implosions, with 3 perturbation scenarios considered. Section II outlines the background theory and contextualises the enclosed results. Simulation setup details are described in Sec. III. Section IV studies a single cold spike, providing a simple example to elucidate the opposing effects of thermal ablative stabilisation reduction and magnetic tension. Section V models a radiation drive asymmetry, resulting in a realistic time-dependent low-mode asymmetry. Section VI uses a multi-mode perturbation to explore the impact of magnetic fields on short-wavelength asymmetries; the prevalence of a short-wavelength structure is increased with thermal magnetisation, while magnetic tension prevents small-scale vortices from forming.

II. BACKGROUND

Magnetised electron heat-flow takes the form[7]

$$\underline{q}_{\kappa} = -\kappa_{\parallel}\hat{\underline{b}}(\hat{\underline{b}}\cdot\nabla \mathrm{T}_e) - \kappa_{\perp}\hat{\underline{b}}\times(\nabla \mathrm{T}_e\times\hat{\underline{b}}) - \kappa_{\wedge}\hat{\underline{b}}\times\nabla \mathrm{T}_e, \quad (1)$$

where $\kappa_{\parallel}$ and $\kappa_{\perp}$ are thermal conductivities parallel and perpendicular to the magnetic field lines. $\kappa_{\wedge}$ is the Righi-Leduc thermal conductivity and $\hat{\underline{b}}$ is the magnetic field unit vector. $\kappa_{\perp}$ decreases with increasing magnetisation, while $\kappa_{\parallel}$ is independent of the field strength. The magnetisation is quantified using the Hall parameter[8]

$$\omega_e\tau_e = 0.096\frac{\mathrm{T}_e[keV]^{3/2}|\underline{B}[kT]|}{n_e\left[10^{25}/cm^2\right]\lambda Z_{eff}}, \quad (2)$$

where τ_e is the electron-ion collision time, ω_e is the electron gyrofrequency, λ is the Coulomb logarithm, and Z_{eff} is the effective ionisation of the plasma. Conceptually, the product of τ_e and ω_e is the expected number of orbits an electron takes (perpendicular to the magnetic field) before each collision. The dependence of $\kappa_{\perp}$ on the Hall parameter was calculated by Epperlein and Haines.[9] $\omega_e\tau_e = 1$ reduces the perpendicular thermal conductivity in a hydrogen plasma by approximately 2/3, i.e., $\kappa_{\perp}(\omega_e\tau_e = 1)/\kappa_{\parallel} \approx 1/3$. A plasma with a Hall parameter of 10 is considered extremely magnetised, with $\kappa_{\perp}(\omega_e\tau_e = 10)/\kappa_{\parallel} \approx 0.01$.

As plasma magnetisation results in anisotropic heat-flows parallel and perpendicular to the magnetic field, implosion symmetry is inherently broken. Even an ideal unperturbed spherical implosion must be simulated at least in 2-D when a magnetic field is imposed.[10] With the magnetic field applied along z, spherical polar co-ordinates r and θ are used throughout this paper, although the single-spike (Sec. IV) and multi-mode (Sec. VI) simulations here are 3-D in nature, incorporating variations in ϕ.

The effect of heat-flow magnetisation on the hot-spot energy containment and shape has been studied using simulations previously,[1,6,10] with repeated observations of hot-spot elongation along the magnetic field lines. The work in this paper builds upon this by using various perturbation scenarios, including 3-D asymmetries and perturbations based on experimental observables.

The Righi-Leduc heat-flow [the term in Eq. (1) associated with $\kappa_{\wedge}$] acts perpendicular to both the magnetic field and the temperature gradient. For an unperturbed capsule simulated in 2-D, this sends a heat-flow in ϕ. For a strictly 2-D implosion, this does not change the thermal energy distribution (as $\nabla\cdot\underline{q}_{Righi} = 0$).[10] 3-D perturbations are required for the Righi-Leduc heat-flow to change the capsule energy containment. While 3-D simulations are considered here, the effect of Righi-Leduc is of secondary importance, as $\kappa_{\wedge}$ is small during the capsule stagnation phase for the large hot-spot magnetisations observed. This is in contrast to hot-spots without an applied external magnetic field, where the magnetic flux is expected to be self-generated by the Biermann Battery mechanism; Righi-Leduc can be an important heat-loss process in these moderately magnetised ($\omega_e\tau_e \approx 1$) hot-spots.[11]

The Lorentz force from a magnetic field onto a plasma is given by

$$\underline{F}_{Lorentz} = \frac{1}{2\mu_0}(\underline{B}\cdot\nabla)\underline{B} - \frac{1}{2\mu_0}\nabla(\underline{B}\cdot\underline{B}). \quad (3)$$

The first term is a magnetic field line tension force, which acts to straighten the field lines. The second term is comparable to a pressure force, where the magnetic pressure is $\mathrm{P}_B = |\underline{B}|^2/2\mu_0$. The thermal and magnetic pressures are traditionally compared using the plasma β

$$\beta = \frac{\mathrm{P}_T}{\mathrm{P}_B} = \frac{2\mathrm{P}_T\mu_0}{|\underline{B}|^2}. \quad (4)$$

While the thermal pressure is always larger than the magnetic pressure in this paper (i.e., $\beta > 1$), the magnetic tension component can dominate the plasma dynamics locally when field lines bend over a small radius. 2-D simulations by Perkins *et al.* demonstrated perturbation growth suppression through pre-magnetisation,[1] although their work suggested that full 3-D calculations including high-mode structures are required to best capture the impact of the Lorentz force on perturbation growth.

High resolution 2-D simulations of the Rayleigh-Taylor-unstable gas-ice interface conducted by Srinivasaan and Tang studied the impact of the Lorentz force on the high-mode structure,[12] finding that high modes are preferentially suppressed (in accordance with linear growth theory[13]). However, thermal conduction was neglected in these simulations, and it is shown in this paper that a careful balance is struck between thermal conduction magnetisation increasing perturbation growth and the Lorentz force decreasing growth rates.

Magnetic fields also change the trajectories of fast charged particles, which is relevant in this paper to the α-particles that are produced through fusion reactions. At birth, a DT-produced α-particle with an energy of 3.5 MeV will be confined to a radius of

$$r_{\alpha}[\mu m] \leq \frac{135}{|\underline{B}[kT]|} \quad (5)$$

although this radius will decrease as the particle slows against the background plasma and deposits its energy. By retaining the α-particles within the hot-spot core, rather than losing them to the cold dense fuel, it is posited that the hot-spot pressure can be greatly enhanced, leading to a high-gain configuration.

Published under license by AIP Publishing

Perkins *et al.* studied the effect of magnetic fields on α-particle heating for NIF experiments.[1,6] High and low-performance implosions were largely unaffected by target magnetisation, while moderate-performance experiments underwent yield enhancement factors of 10–100 as the ignition barrier was passed and α-particle energy coupling to the fuel far exceeded the capsule kinetic energy. A field strength of $B_0 = 50$ T was calculated to be optimal, with larger field strengths reducing the yield due to excessive shape distortion.[1] The current best-performing indirect-drive capsules at NIF are anticipated by Perkins *et al.* to be at the foot of this ignition cliff, providing great motivation for further research.

In order to vary the unmagnetised yields in the parameter scan, Perkins *et al.* systematically reduced the capsule kinetic energy in accordance with the hypothesis that significant residual kinetic energy exists within NIF hot-spots at stagnation.[1] The simulations in this paper build upon the work by Perkins *et al.* by using a perturbation source (time-dependent radiation asymmetry) that was expected to be the dominant yield degradation mechanism for the high-foot shot simulated (N130927).[14,15] While the yield in this case is found to double by the application of a 50 T magnetic field, the amplification factor is expected to be highly dependent on the initial unmagnetised implosion performance. As Perkins *et al.* demonstrated, the amplification factor for current experiments is greater if the unmagnetised implosion yield is higher. The experiment modelled in this paper is from the high-foot campaign, so it has only moderate performance compared with the newer HDC designs.[16]

Large magnetic field strengths are required for thermal magnetisation, the Lorentz force, or α-particle magnetisation to be significant in an ICF hot-spot. To reach a Hall Parameter of 1 (where perpendicular thermal conductivities are reduced by 2/3) in the core of a typical hot-spot ($\rho = 45\,000\,\mathrm{kg/m^3}$ and $T_e = 5000$ eV) requires fields of around 2×10^3T. Magnetised Rayleigh-Taylor growth theory[13] estimates that a field of 10^4 T is required to suppress perturbations of wavelengths 1 μm and smaller in a similar hot-spot, which is the lowest cell size used for the calculations in this paper. For a hot-spot radius of 30 μm, Eq. (5) estimates that α-particles will be contained for a field strength of 4500 T. Magnetic fields of this high intensity cannot be directly generated in a laboratory. However, as the capsule implodes, the magnetic field is (to first order) frozen to the highly conductive plasma and is compressed as the fuel stagnates.

Nernst advection also transports the magnetic field, moving flux down temperature gradients. While this effect is important during the drive-phase,[10] the large plasma magnetisation during stagnation suppresses the Nernst hot-spot demagnetisation.

III. SIMULATION SETUP

Capsule-only simulations are performed using the 3-D radiation extended-magnetohydrodynamics code Gorgon,[11,17] which uses the same framework as in the Chimera code.[14] The radiation transport is non-diffusive, using $P_{1/3}$ automatic flux limiting. Full radiation transport is only used during the 2-D drive-phase simulations, while an optically thin radiative loss model is used here for the 3-D capsule stagnation phase to lower computation time.[18]

Magnetic transport in Gorgon uses the Braginskii formulation[7] with the transport coefficients calculated by Epperlein and Haines.[9] Advection with bulk plasma motion, resistive diffusion, Nernst, Biermann Battery generation of magnetic fields, cross-gradient-Nernst, and Hall transport (with collisional corrections) are all included. The first 3 of these terms are dominant in the parameter regime of interest in this paper.

The full conductive heat-flow from Eq. (1) is used. The $\kappa_\parallel$ and $\kappa_\perp$ terms are more easily incorporated into Chimera by using the vector identity $\underline{C} \times \underline{D} \times \underline{E} = (\underline{C} \cdot \underline{E})\underline{D} - (\underline{D} \cdot \underline{E})\underline{C}$

$$\underline{q}_\kappa = -\kappa_\perp \nabla T_e - (\kappa_\parallel - \kappa_\perp)\hat{\underline{b}}(\hat{\underline{b}} \cdot \nabla T_e) - \kappa_\wedge \hat{\underline{b}} \times \nabla T_e. \quad (6)$$

The first term labels the isotropic thermal conduction $\kappa_{iso} = \kappa_\perp$, as it is independent of the magnetic field direction. The isotropic conduction is incorporated into the code in the same way as unmagnetised conduction is typically treated but using $\kappa_\perp$. The second term is then the anisotropic component $\kappa_{aniso} = \kappa_\parallel - \kappa_\perp$, which adds extra heat-flow along the field lines to represent the lack of thermal magnetisation in this direction. Careful treatment of this term is required to reduce numerical diffusion across the magnetic field lines. The centred-symmetric algorithm outlined by Sharma and Hammett[19] is used, which calculates the heat-flow along magnetic field lines at the cell corners before resolving to the cell faces. Testing of this algorithm includes the diffusion of a hot region of plasma around an intense circular magnetic field.[19,20] The final term in Eq. (6) is the Righi-Leduc heat-flow, which is similarly implemented at the cell corners, but is small during the highly magnetised capsule stagnation phase. The thermal conduction uses a super-stepping scheme[21] to reduce the number of sub-cycles needed for numerical stability, thereby decreasing the simulation runtime. This scheme uses a Runge-Kutta method based on the recursion sequence for Legendre polynomials.[22]

Fusion-produced α-particles are treated using a PIC method.[23] The stopping power model used is from Maynard-Deutsch[24] with the Zimmerman parameterisation.[25] The trajectories are modified by the magnetic field using a Boris push algorithm.[26] Tests have been conducted to find the maximum step-size for magnetised α-particle propagation such that both the magnetic moment and total kinetic energy are conserved throughout the orbit.

Simulations in this paper use high-foot shot N130927, which was an experiment with a yield of 4.4×10^{15}.[15] Estimates place this experiment at the ignition cliff foot, with hot-spot self-heating through α-particle deposition doubling the yield.[2]

All simulations here are initialised in 2-D spherical geometry with the magnetic field along z in the simulation plane. The grid resolution at this stage is 1 μm radially and 1° in the polar direction. The prescribed 2-D time-dependent radiation drive asymmetry[14] is incorporated from the beginning of the drive-phase. Magnetic field effects on the hohlraum (which can affect the radiation asymmetry[27,28]) are not considered here. At 15.7 ns, which corresponds to the peak radiation temperature, the 2-D simulations are reconstructed into 3-D Cartesian for the

Published under license by AIP Publishing

stagnation phase. The grid resolution is then 2 μm for the low-mode asymmetry calculations and 1 μm for the multi-mode.

The single spike and multi-mode perturbations are added artificially before the capsule begins to decelerate, as their evolution with an imposed magnetic field is inherently 3-D. These take the form of velocity perturbations in the ablator, which replicate Rayleigh-Taylor growth.[18,29] While the amplitude, wavelength, and placement of these perturbations are not based directly on specific perturbation sources, ICF implosions are inherently 3-D with surface-roughness and the capsule fill-tube as likely culprits.[15]

A synthetic primary neutron diagnostic is used to infer the hot-spot ion temperature from the emitted neutron energy spectra.[30] The Doppler broadening contribution to the inferred temperature due to plasma bulk flow is neglected, although this effect varies little with magnetisation.

Three externally applied field strengths (B_0) are used throughout this paper:

- 0 T: Unmagnetised base case.
- 5 T: Compressed previously in an ICF implosion,[4] with evidence of thermal conduction suppression through increased hot-spot temperatures.
- 50 T: Estimated to be optimum for increasing NIF yields.[1,6] At this initial field strength, the α-particle trajectories during stagnation are significantly modified.

IV. SINGLE SPIKE

A localised spike or jet is the simplest perturbation scenario used in this paper. A large isolated spike exhibits a similar behaviour to a fill-tube perturbation, sending a jet of cold material across the hot-spot core, albeit without any fine-scale structure. As the magnetic field is most easily applied down the hohlraum axis, the fill-tube propagation direction is perpendicular to the magnetic field. This simulation provides an intrinsically 3-D pre-magnetised target scenario.

Figure 1 shows the magnetic streamlines at peak neutron output for a 5 T single-spike simulation. As the spike pushes into the hot-spot, the field lines predominantly move with the flow, bending around the spike tip. Larger flux compression is seen at the hot-spot centre due to the spike, increasing up to 10 000 T. The topology of these field lines then becomes important for the thermal conduction (reduced only perpendicularly), magnetic tension (acting to straighten the field lines), and the α-particle trajectories (only confined perpendicular to the field lines). These separate magnetisation effects will now be introduced individually, such that the total integrated effect of the magnetic fields should become clear.

A. Magnetised thermal conduction

In this section, the Lorentz force and α-particle production are turned off in the code, such that the effect of thermal conduction modifications can be isolated.

First, the unmagnetised case is considered. As the cold spike pushes into the hot-spot, the perturbation acts as a heat sink. Thermal energy is lost to the cold spike, increasing the surface temperature and ablating some of the spike mass into the hot-spot. The perturbation penetration depth is decreased for two reasons: there is less cold spike mass and the spike surface ablation results in a reaction force pushing against the spike, slowing its propagation. In this way, thermal conduction acts to cool the hot-spot and also decreases deformation through thermal ablative stabilisation.

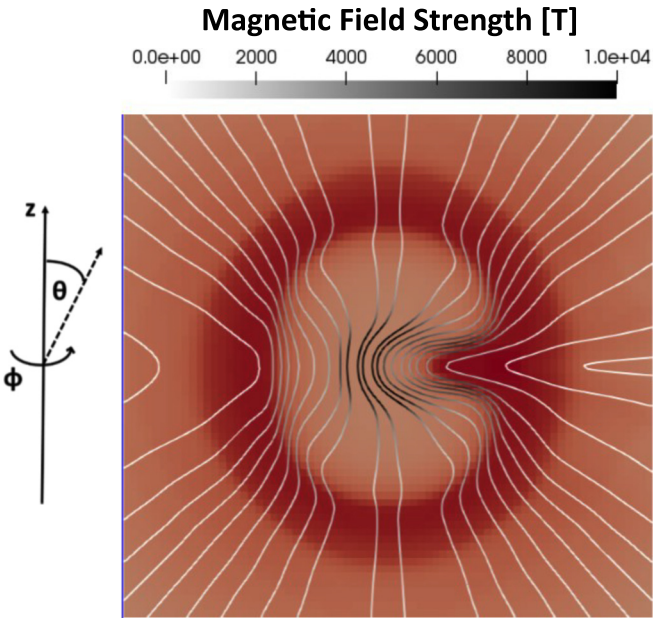


FIG. 1. Magnetic field streamlines coloured by intensity overlaying the hot-spot density at peak neutron output for a $B_0 = 5$ T single-spike simulation. The spike perturbs the magnetic field distribution, bending the field lines around itself. Note that the simulation is 3-D and therefore not symmetric in ϕ.

As a magnetic field is applied to the single-spike simulations, the total hot-spot heat loss decreases, giving a larger hot-spot temperature. The time-integrated neutron-inferred ion temperature increases by 700 eV in the 5 T case and 1200 eV in total for 50 T. Simultaneously, the thermal magnetisation decreases the ablation of cold fuel into the hot-spot, lowering the total hot-spot mass. The hot-spot mass above 1 keV at bang-time decreases from 1.13×10^{-8} kg for 0 T to 1.00×10^{-8} kg for 5 T and 0.94×10^{-8} kg for the 50 T case. The neutron yield increases with magnetisation, from 3.3×10^{15} to 4.2×10^{15} and 4.6×10^{15}.

While the magnetic flux continues to be compressed throughout the burn pulse, the plasma magnetisation actually decreases with time, as the hot-spot cools and becomes more dense [see Eq. (2)]. Note that a plasma magnetisation of $\omega_e\tau_e = 1$, which reduces the perpendicular thermal conductivity by 2/3, does not necessarily result in a 2/3 reduction in perpendicular heat flows. Instead, the higher temperature of the magnetised hot-spot results in steeper temperature gradients across the magnetic field lines, which lead to heat-flows of similar magnitude to those found in the unmagnetised case. For this reason, $\omega_e\tau_e \gg 1$ is needed to thermally insulate an ICF hot-spot.

Figure 2 shows the hot-spot shapes for different applied field strengths at peak neutron output, as well as the isotropic

Published under license by AIP Publishing

and anisotropic heat-flow magnitudes [see Eq. (6)]. As the applied magnetic field is increased, κ_{iso} decreases, while κ_{aniso} increases. The increase in anisotropy results in more heat flowing to the poles, which elongates the hot-spot along z in Fig. 2. Note that the heat-flow at the capsule centre is magnetised at lower applied-field strengths (as it is hotter and less dense) than the hot-spot edge plasma, which can be seen clearly for the 5 T case in Fig. 2.

Noting the orientation of field lines around the cold spike in Fig. 1, the only heat-flow component into the spike is isotropic. Therefore, as thermal magnetisation increases, there is less heat-flow into the spike (and more heat-flow around the spike). While this increases the hot-spot thermal insulation and improves the yield, thermal ablative stabilisation of the spike is decreased, allowing the spike to penetrate further into the hot-spot and increase capsule deformation. Less of the cold fuel spike is heated, lowering the mass of cold spike that is ablated into the hot-spot. This behaviour can be seen in Fig. 2.

Naturally, the choice of spike amplitude and wavelength is important for the quantitative findings in this section. Considering that the analytical growth rates for Rayleigh-Taylor modes are most affected by thermal conduction for smaller wavelengths,[31] it is expected that the change in deformation due to reduced thermal ablative stabilisation will affect these short-wavelength modes most significantly. Section VI uses short-wavelength perturbations to test this hypothesis.

The Rayleigh-Taylor growth is also affected by the density length-scale at the ablation front. As the temperature gradient steepens by reduced thermal conductivities, so does the density gradient, giving a more unstable system. However, analytical models (described in more detail in Sec. VI) suggest that the thermal ablative stabilisation modifications are more dominant in this regime.

B. Lorentz force

Now, the Lorentz force is considered in combination with the magnetisation of thermal conduction.

From Eq. (3), it is clear that the Lorentz force scales strongly with the externally applied field strength. For all applied field strengths in this paper, the plasma β [Eq. (4)] is greater than 5 everywhere, suggesting only a moderate impact. Indeed, for $B_0 = 0$ T and 5 T, there are no noticeable changes to the implosion from the Lorentz force. For $B_0 = 50$ T, however, the single spike is observed to penetrate less deeply into the hot-spot.

The plasma β assumes that the thermal and magnetic pressure lengthscales are the same. This is misleading, as Fig. 1 shows that the magnetic field is bent around the spike tip. The second term in Eq. (3) is a magnetic field tension term and directly opposes any field line bending. The force is then expected to scale as

$$F_{Lorentz} \sim \frac{|\underline{B}|^2}{\mu_0 l_{spike}} \sin\psi, \tag{7}$$

where l_{spike} is the perturbation wavelength and ψ is the angle between the spike propagation direction and the magnetic field.

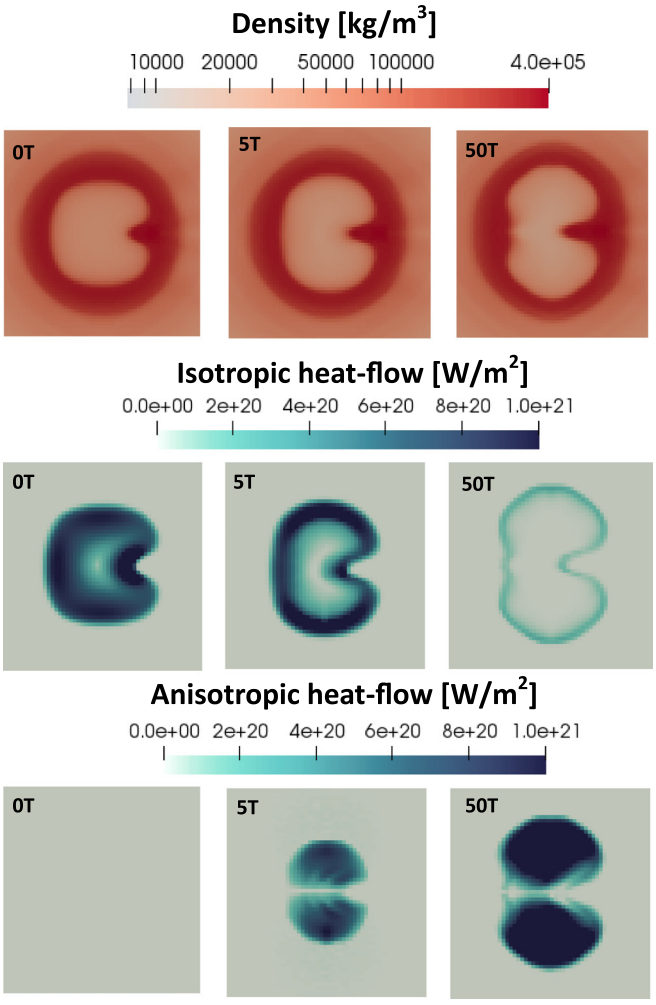


FIG. 2. Density at peak neutron output for single spike simulations with 0 T, 5 T, and 50 T initial magnetic fields applied. The isotropic and anisotropic heat-flow components are also shown. As the applied magnetic field strength increases, the isotropic thermal conduction is suppressed, lowering the thermal ablative stabilisation and allowing the spike to penetrate further into the hot-spot. Simultaneously, the anisotropic heat-flow component is increased, elongating the hot-spot along z.

Figure 3 shows the 1 keV ion temperature contours at peak neutron output for the 0 T, 5 T, and 50 T applied field strengths, including both the magnetised thermal conduction and the Lorentz force. The 0 T and 5 T simulations remain unchanged by the inclusion of the Lorentz force, with the spike penetration depth increasing as the thermal conduction into the spike is magnetised and less thermal ablative stabilisation occurs. From 5 T to 50 T, however, the spike penetration depth decreases, as the Lorentz force acts against the spike penetration. In fact, the reduced thermal ablative stabilisation actually increases the Lorentz force contribution, as it enhances the field line bending around the spike tip. For this reason, including the Lorentz force without magnetised thermal conduction would underestimate the importance of magnetic tension.

Published under license by AIP Publishing

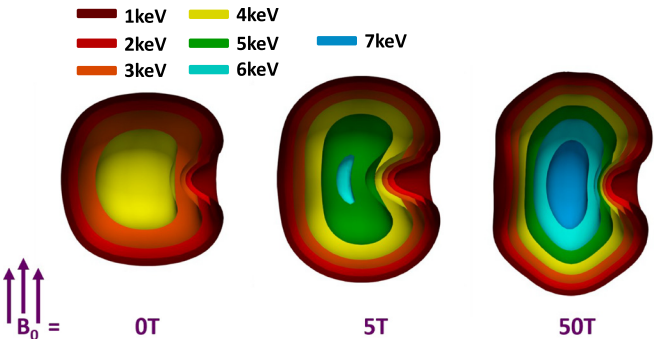


FIG. 3. Cuts through hot-spot ion temperature contours at 1 keV intervals for the single-spike simulations at peak neutron output. The Lorentz force and thermal magnetisation effects have been taken into account. As the field strength increases, the peak temperature increases and the hot-spot elongates along the field lines. While the spike penetration depth increases between the 0 T and 5 T cases (due to reduced thermal ablative stabilisation), the spike penetration then decreases again between 5 T and 50 T due to the Lorentz force stabilising the perturbation.

From Eq. (7), it is clear that shorter-wavelength spikes are more readily suppressed by the Lorentz force than larger length-scale deformations. Therefore, for a given applied field strength, longer-wavelength spikes are expected to penetrate further into the hot-spot before the Lorentz force dampens their growth. Clearly, a larger magnetic field strength will also damp the perturbation propagation faster.

C. Magnetised α-particle trajectories

To make clear how magnetising α-particle trajectories changes the hot-spot burn (rather than how magnetising thermal conduction changes hot-spot burn), the α-particle trajectories are switched between unmagnetised (travelling in straight lines) and magnetised (travelling in orbits) for this section. The focus is on the $B_0 = 50$ T case, as for $B_0 = 5$ T, the impact of magnetic fields on the α-particle trajectories is negligible.

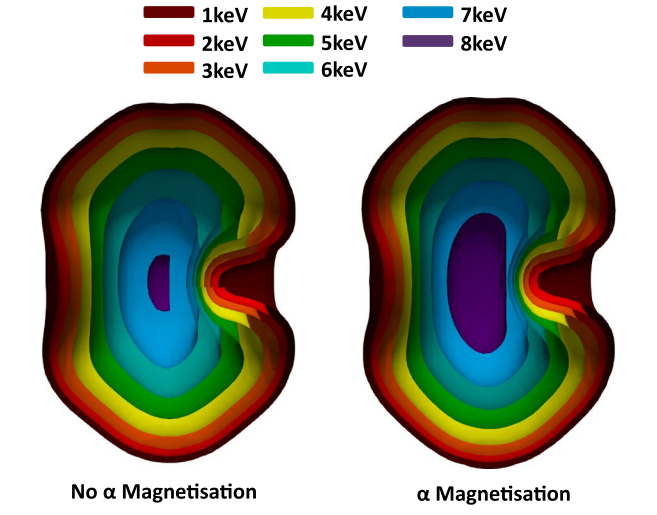


FIG. 4. Slices through hot-spot ion temperature contours (1 keV intervals) at the time of peak neutron output for $B_0 = 50$ T simulations without (left) and with (right) α-particle trajectories being affected by the magnetic field. While the peak temperature is increased due to α-particle containment in the core, there is no change in the perturbation penetration depth.

Figure 4 shows 2 sets of pre-magnetised single-spike results, where the only difference is that in the results on the right, the α-particle trajectories are allowed to be influenced by the magnetic field. By increasing the containment of α-particles in the hot-spot, the magnetic field raises the ion temperature and the yield increases by 8%. At birth, the α-particles directed perpendicular to the magnetic field have a Larmor radius as low as 1 μm. However, α-particles initially directed along the applied magnetic field axis are uncontained and can escape. Here, hot-spot elongation actually helps with energy containment, as there is more hot-spot areal density along z for the α-particles to pass through before they deposit their energy outside of the hot-spot. The hot-spot temperature weighted by the α-particle deposition is increased from 3800 eV to 4400 eV when the magnetisation of α-particle trajectories is taken into account. This further makes clear why the peak temperature in Fig. 4 is higher with α-orbit magnetisation switched on in the code: the α-particles stay within the hot core. The core hot-spot has a lower stopping-power than the surrounding fuel (as it is hotter and lower density), so the average distance that an α-particle travels before it thermalises with the background plasma is increased by 23% through magnetisation.

While magnetisation of the α-particle orbits increases the energy containment and yield, the effect on the perturbation propagation in Fig. 4 is negligible. Therefore, the subsequent perturbation types analysed will focus on their modification by the magnetised thermal conduction and the Lorentz force.

Note that thermal conduction suppression decreases the stopping power of the α-particles, as the hot-spot becomes hotter and less dense.[23] This underlines the importance in pre-magnetised experiments of magnetising the α-particle trajectories to confine the self-heating and meet the conditions required for hot-spot ignition.

V. RADIATION ASYMMETRY

For the high-foot experiment simulated, the dominant yield degradation mechanism is expected to be a radiation drive asymmetry.[15] The perturbation is applied in the simulation using a time and frequency-dependent radiation spectrum, where the dominant perturbation is a P4 Legendre-mode.[14] Without a magnetic field, major deformations from spherical symmetry only occur during the stagnation-phase, when non-uniform drive and non-radial kinetic energy effects become amplified by convergence. Spikes form at the capsule poles pushing into the hot-spot, while at the waist, a disk of cold fuel constricts around the burning plasma. After peak neutron output, the non-radial kinetic energy seeded throughout the drive-phase manifests as vorticity within the lobes.[14] Note that the perturbation is symmetric in ϕ, making the simulation 2-D. The unmagnetised case has been studied in depth by McGlinchey *et al.*[14]

Figure 5 shows the magnetic field lines at two times during the stagnation of a capsule with a 5 T applied magnetic field. At

Published under license by AIP Publishing

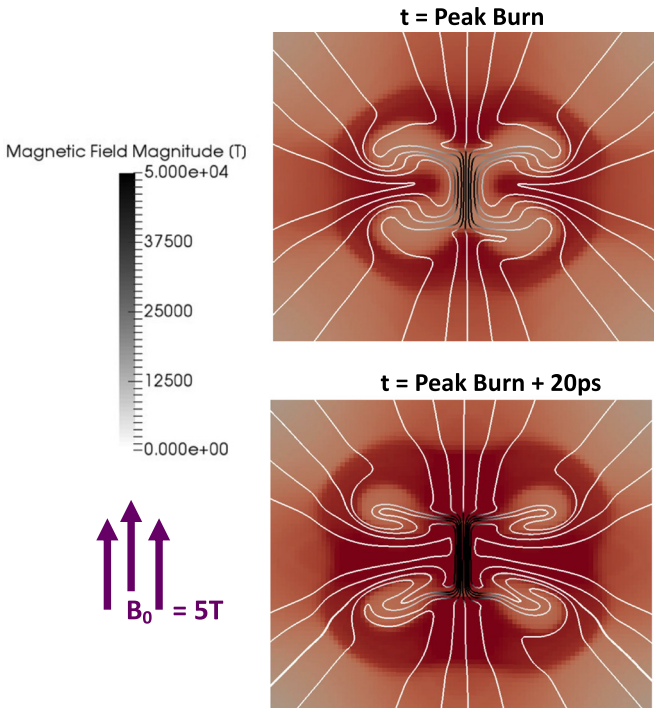


FIG. 5. Magnetic field streamlines at two times near peak neutron output for a capsule perturbed with a P4-dominated time-dependent radiation asymmetry with a 5 T externally applied magnetic field. The streamlines are laid over the density distribution. The perturbation at the capsule waist bends the field lines, much like for the single-spike perturbation discussed in Sec. IV. However, as the simulation is symmetric in ϕ, the field at the capsule centre becomes trapped in an intense column. At later times, the vorticity in the lobes of the P4 perturbation twists the magnetic field lines, enhancing the intensity.

peak neutron output, the streamline deformation resembles the effect observed for the single-spike perturbation in Sec. IV. The plasma constricting around the waist deforms the magnetic field lines, resulting in the field line bending. In this case, however, the perturbation is symmetric in ϕ, and the field piles up in the capsule centre, being amplified into a single column.

At later times, Fig. 5 shows vorticity in the P4 lobes twisting the magnetic field. The energy containment is enhanced by this twisting because both the field strength and the path length for thermal energy along the field lines to the cold fuel are increased.

The effect of thermal conduction magnetisation is initially isolated from the impact of other magnetisation effects. The Lorentz force and magnetisation of α-particle trajectories are only important in the $B_0 = 50$ T case and will be explored subsequently.

Figure 6 shows the change in hot-spot density distribution from thermal conduction magnetisation. As in the single-spike case considered in Sec. IV, magnetisation at the waist reduces the heat-flow into the perturbation locally, which lowers the level of thermal ablative stabilisation, and the perturbation penetrates deeper. However, a contrasting effect is observed at the capsule poles. While the thermal conductivity along the field lines is unchanged by the electron population magnetisation, this heat-flow component is observed to increase with applied field strength. The reduced heat flow at the capsule waist increases the core hot-spot temperature, which increases the electron temperature gradient along z, driving a larger heat-flow along the magnetic field lines. This effect actually increases the thermal ablative stabilisation at the poles, in direct contrast to the effect at the waist.

Figure 7 shows the equivalent $B_0 = 50$ T density slice as in Fig. 6 but with the Lorentz term on. Without the Lorentz force, the cold disk constricts tightly around the hot-spot waist, almost severing the burning plasma into two. When the Lorentz force is taken into account, the perturbation is allowed to grow (and bend the field lines) until a point where the Lorentz force stabilises the perturbation growth.

The magnetic field line distribution in Fig. 5 shows the evidence of fluid vorticity bending the field lines in the P4 lobes. Magnetic tension reduces this vorticity when the capsule is highly magnetised.

The $B_0 = 50$ T target yield is increased by 60% through the Lorentz force alone. Without magnetic pressure and tension in the simulations, the key hot-spot degradation mechanism is through the hot-spot severing into two, truncating the burn pulse. With the Lorentz force keeping the hot-spot core open,

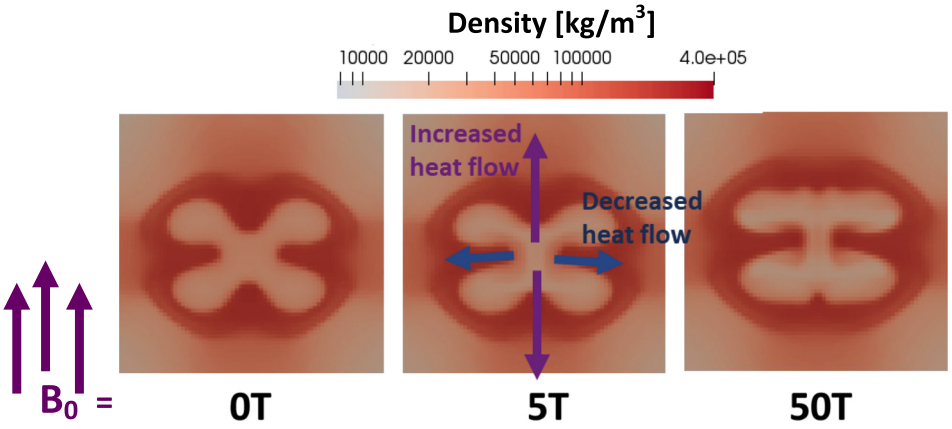


FIG. 6. Density distribution for a capsule perturbed with a time-dependent radiation drive asymmetry for different applied field strengths. The Lorentz force is ignored in these simulations. Heat-flow magnetisation reduces the thermal ablative stabilisation at the capsule waist, increasing the perturbation propagation. The hot-spot also increases in temperature with magnetisation, increasing the unrestricted heat-flow along the field lines towards the poles. This process indirectly increases the thermal ablative stabilisation at the capsule poles, reducing the perturbation propagation.

Published under license by AIP Publishing

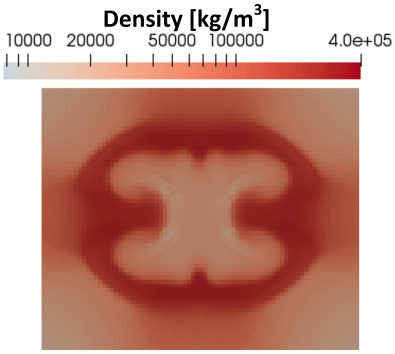


FIG. 7. Density distributions for a capsule with a radiation drive asymmetry and a 50 T applied magnetic field at peak neutron output. The simulation is the same as the 50 T case in Fig. 6 but with the Lorentz force included. The perturbation at the waist bends the magnetic field lines around itself, resulting in a stabilising force lowering the perturbation depth. The Lorentz force here keeps the hot-spot open and results in a larger burn region, increasing the yield by 60%.

as seen in Fig. 7, the burn can continue for longer and the peak of the burn pulse occurs 50 ps later.

Note that when no perturbations are applied to these capsule simulations, the Lorentz force is not significant for any of the initial field strengths used in this analysis. It is only when perturbation propagation bends the field lines over a length scale smaller than the hot-spot radius that the Lorentz force plays a role in a local force balance.

With the α-particle transport switched on, the impact of applying an external magnetic field to the NIF high-foot campaign can be estimated. Figure 8 shows slices through 1 keV ion temperature contours for an unmagnetised radiation drive asymmetry capsule and the same target with a 50 T magnetic field applied. In

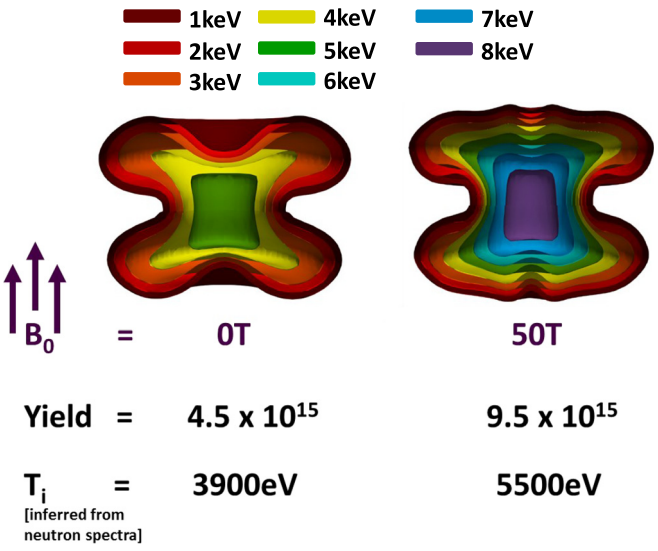


FIG. 8. Cuts through the 1 keV ion temperature contours for the radiation drive asymmetry simulations without and with a 50 T applied magnetic field. The respective yield and ion temperature inferred by the neutron spectra are included.

these simulations, all of the magnetisation effects have been turned on. The yields and neutron inferred ion temperatures are also included within Fig. 8. The hot-spot temperature increases by over 1500 eV due to magnetisation, with the peak ion temperature increasing from 5 keV to 8 keV. Magnetisation has a more moderate impact on the yield (as the hot-spot density is simultaneously decreased) doubling the performance. For comparison, the expected yield amplification factor would be 3.5 for the same temperature increase but keeping the hot-spot density constant. While this high-foot capsule has not been elevated into the ignition regime, it is expected that magnetising a higher base unmagnetised case (such as the more recent HDC capsule implosions[16]) will result in greater yield amplification.

VI. MULTI-MODE

In this section, velocity perturbations of different wavelengths are applied randomly to the capsule at peak radiation temperature,[11,18] with the highest mode limited by the 1 μm simulation cell size. The relative amplitude of the high and low modes is arbitrary, but the total amplitudes are tuned such that the unmagnetised yield matches the experiment. In this way, a highly asymmetric and 3-D capsule with a high-mode structure can be simulated while staying relevant to experiments by matching the yield. Perturbations like these could occur from impurities in the DT ice, surface roughness defects, or the ablator grain structure, which are then amplified by the Rayleigh-Taylor instability during the deceleration phase.

A. Magnetised thermal conduction

The multi-mode simulations are a natural candidate for studying thermal conduction modifications. Short-wavelength perturbations increase the hot-spot surface area for thermal losses, while long wavelengths bring the cool hot-spot surface into contact with the hot core.[18] In combination, the heat loss is the greatest.

Figure 9 shows a cut through ion temperature contours (at a 1 keV interval) for the different magnetic field strengths at the time of peak neutron output. As with the other perturbations considered, the core temperature is increased by reducing the thermal losses at the hot-spot edge. The peak temperature increases from below 5000 eV without an applied magnetic field to 8000 eV for $B_0 = 50$ T. The increased temperature is observed throughout the burn pulse. In addition, the hot-spot is observed to elongate along the magnetic field lines. Decreased thermal ablative stabilisation is also seen at the capsule waist, with the hot-spot being narrower for larger field strengths.

An instantaneous magnetised thermal conduction reduction factor χ can be defined as the ratio of heat lost from the hot-spot to what it would be if the plasma magnetisation is neglected (for the same temperature-density profile)

$$\chi = \frac{\iiint_V \nabla \cdot \underline{q} dV}{\iiint_V \nabla \cdot \underline{q}(\omega_e \tau_e = 0) dV}. \quad (8)$$

In this section, the hot-spot is taken as the heat-source hot-spot, which is defined as the hot-spot volume which loses

Published under license by AIP Publishing

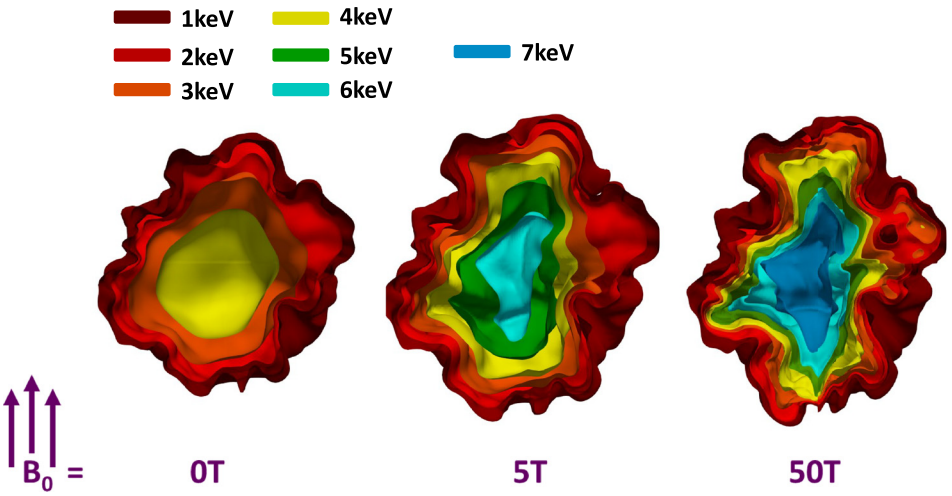


FIG. 9. Ion temperature contours (1 keV intervals) at the peak neutron output for different applied magnetic field strengths. Only heat-flow magnetisation is taken into account. Larger magnetisation increases the energy containment and raises the hot-spot temperature. Increased heat-flow along the magnetic field lines elongates the hot-spot. Higher-mode perturbations are observed in the highly magnetised case, with modes that are thermally stabilised for $B_0 = 0$ T allowed to grow for $B_0 = 50$ T.

the greatest power by thermal conduction. The plasma surrounding the heat-source hot-spot is gaining more thermal energy from the heat-source hot-spot than it is losing to the rest of the plasma.

For the 50 T case, $\chi = 0.1$ at the time of peak neutron output, suggesting that the thermal magnetisation reduces the heat-source hot-spot energy losses by 90%. This is surprisingly large, as the magnetic field only reduces the heat-flow perpendicular to itself. Previous 1-D calculations have approximated the effect of extreme magnetisation by reducing heat-flows by 50%.[4] Such low values of χ show that the hot-spot elongation feature helps to increase the thermal insulation by increasing the path length along the field lines from the hot-spot core to the cold surrounding fuel.

Figure 9 also suggests that large magnetic fields increase the presence of high-mode deformations on the hot-spot surface. It is well-understood that high-mode asymmetries are preferentially suppressed by unmagnetised thermal conduction.[31] The highest Rayleigh-Taylor modes are expected to be completely inhibited by thermal ablative stabilisation without a magnetic field. By reducing the thermal conductivities at the instability growth front, magnetisation of the hot-spot heat-flow allows higher-modes to grow.

B. Lorentz force

The variety of mode numbers used in this simulation provides another useful configuration to examine the Lorentz force. The magnetic force results in two key modifications for the $B_0 = 50$ T case. Firstly, the cold fuel constriction around the hot-spot waist (which is enhanced by reduced thermal ablative stabilisation) is reduced, as was seen for the radiation asymmetry case. Secondly, vortices are suppressed by magnetic tension.

The magnetic field distribution for the multi-mode perturbation is highly disordered. The peak field is observed at a "bottleneck," with the cold fuel at the waist constricting around the hot-spot centre, as seen in the other perturbation scenarios. At this central location, the field strength is amplified to as high as 10^5 T.

Figure 10 shows a density slice through the 3-D simulations without and with the Lorentz force included. As in the radiation asymmetry case, bending of the magnetic field at the waist due to cold fuel propagation results in a radial tension force, which is able to stabilise the perturbation and keep the hot-spot relatively open. This allows the hot-spot to burn for longer, and the time of peak neutron production is moved later by 20 ps.

Now, attention is turned to the high-mode behaviour, which is specific to the multi-mode simulations. Figure 10 shows the presence of vortices (pointed out by arrows) when the Lorentz force is not included. As the vortices roll over, they amplify the field locally through a twisting action. These vortices are suppressed by the magnetic tension force, which acts to straighten the field lines and reduce vorticity. The Lorentz force makes the hot-spot edge smoother, reducing some of the high-mode structure.

Analytical linear 2-D Rayleigh-Taylor stability analysis without thermal conduction suggests that a critical in-plane magnetic field strength B_c is required to suppress a perturbation of wavelength λ[12,13]

$$B_c > \sqrt{\mu_0(\rho_h - \rho_l)g\lambda}, \tag{9}$$

where ρ_h and ρ_l are the heavier and lighter fluids in the Rayleigh-Taylor unstable system with the lighter fluid accelerating into the heavier fluid at g. Using the values of ρ_h, ρ_l, and g estimated from the multi-mode simulations, the theoretical critical magnetic field strength to suppress a perturbation on the order of the grid size (1 μm) and below is greater than 10^4 T. This agrees reasonably well with the 3-D simulations, where the $B_0 = 5$ T case remains unaffected by the Lorentz force (the field strength is less than 10^4 T at the hot-spot edge), while the $B_0 = 50$ T case sees large changes (the field strength is greater than 10^4 T at the hot-spot edge).

It is important to note that vortex suppression in the simulations is not just observed at the capsule waist, where the theory predicts that the field acts to stabilise the perturbation growth. Figure 10 shows that at the poles, vortices are also

Published under license by AIP Publishing

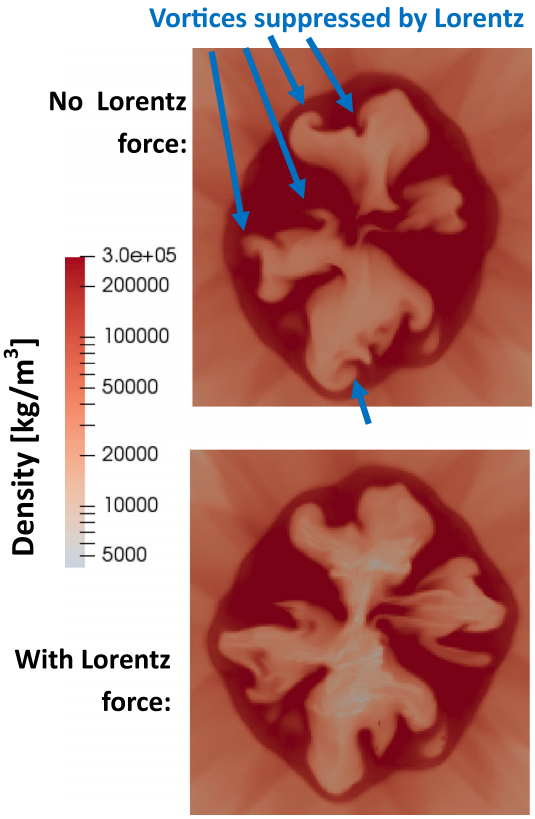


FIG. 10. Multi-mode density slices 50 ps after peak neutron output for a capsule perturbed by multiple modes and with a 50 T applied magnetic field. The top slice is without the inclusion of the Lorentz force. The arrows point to vortices developing at the Rayleigh-Taylor unstable hot-spot edge. The bottom slice includes the Lorentz force, with the vortices being suppressed by magnetic tension.

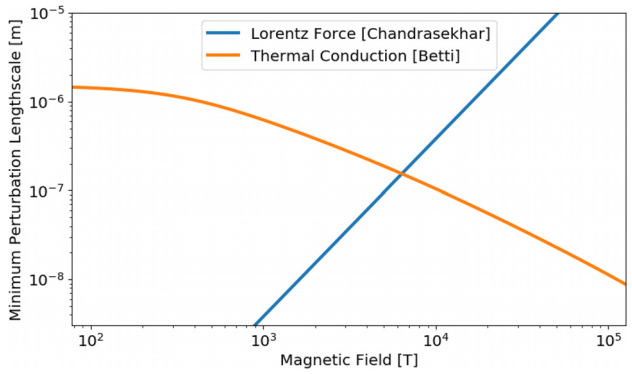


FIG. 11. Theoretical minimum perturbation size as a function of magnetic field strength as dictated by reduced thermal ablative stabilisation (from Betti *et al.*[31]) and by Lorentz force stabilisation (from Chandrasekhar[13]). Rayleigh-Taylor perturbation length scales in unmagnetised capsules are suppressed by thermal conduction. As magnetic fields are applied, thermal conduction stabilisation reduces and the minimum unstable perturbation size also decreases. At larger field strengths, the Lorentz force stabilisation becomes the limiting factor and the minimum perturbation size increases with field strength.

suppressed. This is because vortices form during the Rayleigh-Taylor non-linear growth phase, while the theory is restricted to the linear phase. Physically speaking, any hot-spot surface motion that twists the magnetic field lines will result in a tension force opposing the twist.

In Sec. VI A, it was observed that the minimum perturbation allowed due to thermal ablative stabilisation decreases with thermal magnetisation. Here, it is observed that the Lorentz force acts to suppress these modes. Clearly, there is a competition between these two processes. Theoretical relations from Betti *et al.* and Eq. (9) can be used to understand the behaviour across a range of magnetic field strengths.[13,31]

Betti uses a deceleration-phase model of ICF experiments derived from the hot-spot conservation equations. The ablation velocity at the hot-spot surface is formulated in terms of hot-spot temperature, density, and size. This ablation velocity is then used to alter the hydrodynamic Rayleigh-Taylor growth rate (for a given perturbation wavelength) to incorporate thermal ablative stabilisation.[31] Here, the model is simply extended to use the magnetised thermal conductivity, with an additional input parameter of the magnetic field intensity. Hot-spot parameters are taken from the simulation results at bang-time.

Figure 11 plots the two theoretical relations for the minimum perturbation size against local magnetic field strength.[13,31] For unmagnetised capsules, the small-wavelength perturbations are completely suppressed by thermal ablative stabilisation, with minimum length-scales around the simulation grid size here (1 μm). As the field strength increases, the thermal conduction is suppressed (perpendicular to the magnetic field) and the minimum length scale drops far below the resolution used in the enclosed simulations (as low as 0.2 μm), suggesting that the shortest wavelengths are being artificially suppressed numerically. As the magnetic field strength is increased further, the Lorentz force begins to suppress the highest modes and the minimum perturbation size increases with magnetic field strength. The $B_0 = 50$ T case has a peak field strength at the hot-spot edge of around 40 000 T, suggesting that the minimum perturbation size should be increased by magnetisation to $>5\,\mu$m; the simulations in Fig. 10 at least agree that the minimum perturbation length-scale is limited by the Lorentz force.

VII. CONCLUSION

3-D extended-MHD simulations of pre-magnetised indirect-drive targets have been studied for three perturbation scenarios: a single spike propagating perpendicular to the magnetic field, a low-mode radiation drive asymmetry, and a hot-spot perturbed with both low and high modes. While magnetisation universally increased the target performance, the influence of an applied magnetic field on hot-spot deformation varied.

Moderately magnetised capsules ($B_0 = 5$ T) were dominated by thermal conduction modifications. Perturbations penetrated deeper perpendicular to the field due to reduced thermal ablative stabilisation, while perturbations parallel with the magnetic field were stabilised through increased heat-flows from

Published under license by AIP Publishing

enhanced hot-spot temperatures. For highly magnetised capsules ($B_0 = 50$ T), the Lorentz force was also important, reducing deformation where perturbations had bent magnetic field lines. While magnetisation of α-particle trajectories increased core hot-spot temperatures, there was no impact on perturbation penetration. For higher yield implosions than considered here, where α-particles play a greater role in fire-polishing perturbations,[23] magnetisation of particle orbits is expected to increase in importance, with enhanced hot-spot elongation and decreased perturbation stabilisation perpendicular to the magnetic field likely effects.

These findings inform future design decisions. By placing the fill-tube perpendicular to the magnetic field (which is the most obvious configuration for an indirect-drive experiment), the subsequent perturbation will be maximally affected by plasma magnetisation. These simulations anticipate the fill-tube perturbation penetrating deeper for moderate magnetisation but less deep for a highly magnetised implosion. A negative P2 radiation drive asymmetry could also be purposefully applied to counteract the anisotropic thermal conduction, resulting in a rounder hot-spot at the time of peak neutron production. However, hot-spot elongation has the benefit of increasing the path length along the magnetic field lines for thermal energy and α-particles to escape the hot core, and so, purposefully adjusting for a more symmetric hot-spot may have limited benefit.

Capsule magnetisation will also affect both the dominant Rayleigh-Taylor growth mode and the highest mode that can grow. High modes are particularly detrimental to ICF capsule performance, as they are responsible for mix (increasing radiative losses) and enhance thermal conduction. As pre-magnetisation is increased, the prevalence of high modes is first anticipated to increase due to reduced thermal ablative stabilisation and then decrease as magnetic tension stabilises perturbation growth. For the high-foot experiments simulated, in order to not decrease the minimum perturbation wavelength, an applied magnetic field of at least $B_0 = 25$ T should be used. Any field strength above this is expected to increase the minimum wavelength above the unmagnetised case.

A doubling of the neutron yield is expected by applying an external magnetic field to capsules from the high-foot campaign. While this is a modest increase in the pursuit of ignition, the yield amplification through magnetisation is expected to increase as the α-heating contribution becomes more significant, as is the case in more recent experiments using the HDC ablator.[16] Future work will focus on the accurate modelling of experiments from this campaign to better constrain the potential benefits of external magnetic fields on NIF implosions.

ACKNOWLEDGMENTS

The results reported in this paper were obtained using the UK National Supercomputing Service ARCHER and the Imperial College High Performance Computer Cx1. This work was supported by EPSRC under Grant Nos. EP/K028464/1, EP/M01102X/1, EP/L000237/1, and EP/P010288/1, as well as the Lawrence Livermore National Laboratory Academic Partnership Program and AWE Aldermaston.

REFERENCES

[1]L. J. Perkins, D. D.-M. Ho, B. G. Logan, G. B. Zimmerman, M. A. Rhodes, D. J. Strozzi, D. T. Blackfield, and S. A. Hawkins, "The potential of imposed magnetic fields for enhancing ignition probability and fusion energy yield in indirect-drive inertial confinement fusion," Phys. Plasmas **24**, 062708 (2017).

[2]O. A. Hurricane, D. A. Callahan, D. T. Casey, P. M. Celliers, C. Cerjan, E. L. Dewald, T. R. Dittrich, T. Döppner, D. E. Hinkel, L. F. B. Hopkins, J. L. Kline, S. Le Pape, T. Ma, A. G. MacPhee, J. L. Milovich, A. Pak, H.-S. Park, P. K. Patel, B. A. Remington, J. D. Salmonson, P. T. Springer, and R. Tommasini, "Fuel gain exceeding unity in an inertially confined fusion implosion," Nature **506**, 343–348 (2014).

[3]M. Hohenberger, P. Y. Chang, G. Fiksel, J. P. Knauer, R. Betti, F. J. Marshall, D. D. Meyerhofer, F. H. Séguin, and R. D. Petrasso, "Inertial confinement fusion implosions with imposed magnetic field compression using the OMEGA laser," Phys. Plasmas **19**, 056306 (2012).

[4]P. Y. Chang, G. Fiksel, M. Hohenberger, J. P. Knauer, R. Betti, F. J. Marshall, and D. D. Meyerhofer, "Fusion yield enhancement in magnetized laser-driven implosions," Phys. Rev. Lett. **035006**, 2–5 (2011).

[5]J. P. Knauer, O. V. Gotchev, P. Y. Chang, D. D. Meyerhofer, O. Polomarov, R. Betti, J. A. Frenje, C. K. Li, M. J. E. Manuel, R. D. Petrasso, J. R. Rygg, and F. H. Śguin, "Compressing magnetic fields with high-energy lasers," Phys. Plasmas **17**, 056318 (2010).

[6]L. J. Perkins, B. G. Logan, G. B. Zimmerman, and C. J. Werner, "Two-dimensional simulations of thermonuclear burn in ignition-scale inertial confinement fusion targets under compressed axial magnetic fields," Phys. Plasmas **20**, 072708 (2013).

[7]S. I. Braginskii, "Transport processes in a plasma," Rev. Plasma Phys. (Consultants Bureau, New York, 1965), Vol. 1, pp. 205–311; available at https://scholar.google.com/scholar?hl=en&q=S.+I.+Braginskii%2C+%E2%80%9CTransport+processes+in+a+plasma%2C%E2%80%9D+Reviews+of+Plasma+Physics+%28Consultants+Bureau%2C+New+York%2C+1965%29%2C+Vol.+1%2C+pp.+205%E2%80%93311.

[8]J. D. Huba, NRL *Formulary* (Naval Research Laboratory, Washington, DC, 2013).

[9]E. M. Epperlein and M. G. Haines, "Plasma transport coefficients in a magnetic field by direct numerical solution of the Fokker–Planck equation," Phys. Fluids **29**, 1029 (1986).

[10]J. R. Davies, R. Betti, P.-Y. Chang, and G. Fiksel, "The importance of electrothermal terms in Ohm's law for magnetized spherical implosions," Phys. Plasmas **22**, 112703 (2015).

[11]C. Walsh, J. Chittenden, K. McGlinchey, N. Niasse, and B. Appelbe, "Self-generated magnetic fields in the stagnation phase of indirect-drive implosions on the national ignition facility," Phys. Rev. Lett. **118**, 155001 (2017).

[12]B. Srinivasan and X.-Z. Tang, "The mitigating effect of magnetic fields on Rayleigh-Taylor unstable inertial confinement fusion plasmas," Phys. Plasmas **20**, 056307 (2013).

[13]S. Chandrasekhar and J. Gillis, "Hydrodynamic and Hydromagnetic Stability," (Clarendon Press, 1962), p. 15.

[14]K. McGlinchey, "Diagnostic signatures of performance degrading perturbations in inertial confinement fusion implosions," Phys. Plasmas **25**, 122705 (2018).

[15]D. S. Clark, C. R. Weber, J. L. Milovich, J. D. Salmonson, A. L. Kritcher, S. W. Haan, B. A. Hammel, D. E. Hinkel, O. A. Hurricane, O. S. Jones, M. M. Marinak, P. K. Patel, H. F. Robey, S. M. Sepke, and M. J. Edwards, "Three-dimensional simulations of low foot and high foot implosion experiments on the National Ignition Facility," Phys. Plasmas **23**, 056302 (2016).

[16]S. L. Pape, L. Berzak Hopkins, L. Divol, A. Pak, E. Dewald, S. Bhandarkar, L. Bennedetti, T. Bunn, J. Biener, J. Crippen, D. Casey, D. Edgell, D. Fittinghoff, M. Gatu-Johnson, C. Goyon, S. Haan, R. Hatarik, M. Havre, D. D.-M. Ho, N. Izumi, J. Jaquez, S. Khan, G. Kyrala, T. Ma, A. Mackinnon, A.

Published under license by AIP Publishing

MacPhee, B. MacGowan, N. Meezan, J. Milovich, M. Millot, P. Michel, S. Nagel, A. Nikroo, P. Patel, J. Ralph, J. Ross, N. Rice, D. Strozzi, M. Stadermann, P. Volegov, C. Yeamans, C. Weber, C. Wild, D. Callahan, and O. Hurricane, "Fusion energy output greater than the kinetic energy of an imploding shell at the National Ignition Facility," Phys. Rev. Lett. **120**, 245003 (2018).

[17]A. Ciardi, S. V. Lebedev, A. Frank, E. G. Blackman, J. P. Chittenden, C. J. Jennings, D. J. Ampleford, S. N. Bland, S. C. Bott, J. Rapley, G. N. Hall, F. A. Suzuki-Vidal, A. Marocchino, T. Lery, and C. Stehle, "The evolution of magnetic tower jets in the laboratory," Phys. Plasmas **14**, 056501 (2007); eprint arXiv:0611441 [astro-ph].

[18]S. Taylor and J. P. Chittenden, "Effects of perturbations and radial profiles on ignition of inertial confinement fusion hotspots," Phys. Plasmas **21**, 062701 (2014).

[19]P. Sharma and G. W. Hammett, "Preserving monotonicity in anisotropic diffusion," J. Comput. Phys. **227**, 123–142 (2007).

[20]C. A. Walsh, "Extended magneto-hydrodynamic effects in indirect-drive inertial confinement fusion experiments," Ph.D. thesis, Imperial College London, 2018.

[21]C. D. Meyer, D. S. Balsara, and T. D. Aslam, "A stabilized Runge-Kutta-Legendre method for explicit super-time-stepping of parabolic and mixed equations," J. Comput. Phys. **257**, 594–626 (2014).

[22]C. D. Meyer, D. S. Balsara, and T. D. Aslam, "A second-order accurate super timestepping formulation for anisotropic thermal conduction," Mon. Not. R. Astron. Soc. **422**, 2102–2115 (2012).

[23]J. K. Tong, K. McGlinchey, B. D. Appelbe, C. A. Walsh, A. J. Crilly, and J. P. Chittenden, "Burn regimes in the hydrodynamic scaling of perturbed inertial confinement fusion hotspots" (unpublished).

[24]G. Maynard and C. Deutsch, "Born random phase approximation for ion stopping in an arbitrarily degenerate electron fluid," J. Phys. **46**, 1113–1122 (1985).

[25]G. B. Zimmerman, "Monte Carlo methods in ICF," in *the 13th International Conference on Laser Interactions and Related Plasma Phenomena* (ASCE, 1997), Vol. 406, pp. 23–41.

[26]J. P. Boris, "Relativistic plasma simulation-optimization of a hybrid code," in *Numerical Simulation of Plasmas*, 4th ed. (Washington, DC, 1970).

[27]D. J. Strozzi, L. J. Perkins, M. M. Marinak, D. J. Larson, J. M. Koning, and B. G. Logan, "Imposed magnetic field and hot electron propagation in inertial fusion Hohlraums," J. Plasma Phys. **81**, 475810603 (2015).

[28]D. S. Montgomery, B. J. Albright, D. H. Barnak, P. Y. Chang, J. R. Davies, G. Fiksel, D. H. Froula, J. L. Kline, M. J. MacDonald, A. B. Sefkow, L. Yin, and R. Betti, "Use of external magnetic fields in Hohlraum plasmas to improve laser-coupling," Phys. Plasmas **22**, 010703 (2015).

[29]D. Layzer, "On the instability of superposed fluids in a gravitational field," Astrophys. J. **122**, 1 (1955).

[30]B. Appelbe and J. Chittenden, "Relativistically correct DD and DT neutron spectra," High Energy Density Phys. **11**, 30–35 (2014).

[31]R. Betti, M. Umansky, V. Lobatchev, V. N. Goncharov, and R. L. McCrory, "Hot-spot dynamics and deceleration-phase Rayleigh–Taylor instability of imploding inertial confinement fusion capsules," Phys. Plasmas **8**, 5257–5267 (2001).

Published under license by AIP Publishing